PRECISE MEASUREMENT OF THE SOLAR GRAVITATIONAL RESDHIFT (a proposal to INFN for funding)

by:
Alessandro Cacciani
Fabrizio Massa
Paolo Rapex
Runa Briguglio
………………... Univ of Rome "LA SAPIENZA", Italy
in collaboration with
James LoPresto
………………...Edinboro University of Pennsylvania, USA

Introduction

The reasons why many projects are being conceived concerning sensitive tests of Fundamental Physics, especially General Relativity, are due to both theoretical and experimental aspects. From the theoretical side, the attempt to unify General Relativity and Quantum Theory appears to imply deviations from standard physics; at the same time, exciting progress on precise instrumentations make it possible to plan new measurements able to accomplish new tests and even to open the door to unexpected results. Therefore there is a worldwide effort to push for new technologies, both from the space and on the ground, with the hope to better clarify Quantum Physics and General Relativity or to explore the expectations for "new physics". During the last decades we have been developing a particular technology (worldwide adopted and known with the name of MOF , Magneto-Optical Filter) that is able to measure spectral line shifts with unsurpassed precision and absolute reference stability. Therefore, we can focus our interest on a new measurement of the Solar Gravitational Red Shift that is waiting for more precise determination since the last figure given by LoPresto Shrader and Pierce in 1991 (ApJ 367:757-760). Our aim it to improve such determination (now at the level of some percents) of one order of magnitude, at least. For this, we have contacted Dr LoPresto for detailed information on his work and obtained his welcome desire to join our effort. This proposal is therefore composed of 4 sections: the first one deals with a brief historical overview; the second one is from J.LoPresto himself and describes his latest results; the third section describes our MOF technology and finally, the fourth section describes our envisioned strategy for the measurement.

1.Brief Historical Review

Following the General theory of Relativity, the gravitational potential of a celestial body affect the physical time and slow any periodic phenomenon considered as a physical clock. In order to verify this statement, is therefore needed to compare the behavior of different types of clocks located in different gravitational potentials. A clean experiment conducted by Vessot et al (1980, Physical Rev. Letters , vol 45, N.26, pg 2081) comparing the frequency standard of two Hydrogen Masers, one on the ground and the other at 10000 Km on a spacraft, was able to verify the theoretical prediction at the level of about 10 exp (-4) . A different kind o clock is given by the atomic spectral lines. The solar gravitational potential, for example, shifts their wavelengths relative to the laboratory lines on the Earth, by the amount $\Delta\lambda$= 2.1 x 10 exp(-6) λ towards the red. In terms of velocity, this is equivalent to a Doppler shift of 636 m/s. The solar spectrum is also attractive in this context because the Sun is a massive body bringing the Relativity verification to values far larger than what is possible on Earth (dynamic range). An attempt to measure such a GRS (Gravitational Red Shift) is however complicated by additional effects that can change λ , depending on the line forming layer on the atmosphere of the sun: for ex., lower layers are affected by convective upward gas motions to a large extent (about 12 mA equivalent Doppler blue shift), while higher layers, at the chromospheric levels, appear less affected. A review article is by Dravings (1982 ARAA, 61) Also most of the solar lines are asymmetric, displaying complex bisectors. Therefore, care must be taken to disentangle among various sources of wavelength shifts. Chromospheric lines like the Sodium Doublet, show good symmetry and could be good candidates for the measurement. However they are blended by telluric water vapour lines , particularly D2. The Potassium line @ 770 nm appears to be fairly symmetrical and free from water vapor blends; however it is affected by a convective blue shift. Potassium and Sodium lines have been used to measure the GRS on selected points on the solar disk by Roddier (165, Ann. Ap. 28,463) and Snider (1972, Phys. Rev. Letters, 28, 853)   reaching the precision of about 5%. However, the time dependent velocity fied present on the surface of the sun makes the above measurements very uncertain; for this reason LoPresto, Shrader and Keith Pirce (August 1991, ApJ 367,757)decided to use chromospheric Oxigen lines in emission, that are formed well above the main convective velocity field, reaching the precision of about 2%.
This proposal deals with the solar GRS with the aim to improve its precision to a level comparable with the measurement of Vessot et al

Latest Results

(from LoPresto)

Alessandro Cacciani, his colleagues and I are attempting to improve upon the measurements of the Gravitational Red Shift made by myself and A. Keith Pierce using the main spectrograph of the McMath-Pierce Solar Telescope in 1991 (Ap 367, 757). We will use the Magneto-Optical Filler (MOF) in conjunction with one of the auxiliary beams of the McMath-Pierce Solar telescope at Kitt Peak Arizona.

In 1991, Keith Pierce and I used the potassium near infrared triplet at a wavelength of about 779 nanometers. We observed these lines in the solar photosphere and in the flash spectrum at the edge of the chromo sphere along with comparison lines of the same transition using a hollow cathode tube. The chromospheric flash spectra provided highly symmetrical lines for relatively easy wavelength measurements. We constructed bisectors for the absorption lines on the disc, which we observed from disc center to limb and extrapolate the Doppler shift to the limb of the disc. Our measurements resulted in a value of 0.99 of the predicted value with about a 1-2% internal error.

We feel confident that we can improve upon this value using the MOF system.

3. The MOF Technology

In the figures below we show selected pictures of the Sun taken with our Magneto-Optical Filter (MOF). This is an easy way to illustrate the instrument performances and will become clearly understood after the following description of the MOF working principle.
For a comprehensive theoretical and experimental study of the MOF , please refer to the Appendix. Here we give brief outlines.

In Fig.1 our instrument is shown as composed by three parts (a telescope, the MOF filter and an image sensor). Fig.2 shows its practical realization on the roof of our Institute in Rome. Indeed, the MOF is the core of the system that makes this experiment unique. Its working principle is fully described in Appendix. Here let be enough to say that it is a very stable and narrow double band filter. The two bands could be as narrow as 50 milliAngstrom (see Fig 3), achieving unsurpassed performances as far as its central wavelength reference stability and symmetrical tuning in the wings of the solar lines (Red and Blu sides). Each band can be selected separately at will so that a computer comparison (difference) between the transmitted images produces the wanted Doppler image of Fig 4.A single band gives an intensity image like in Fig.5

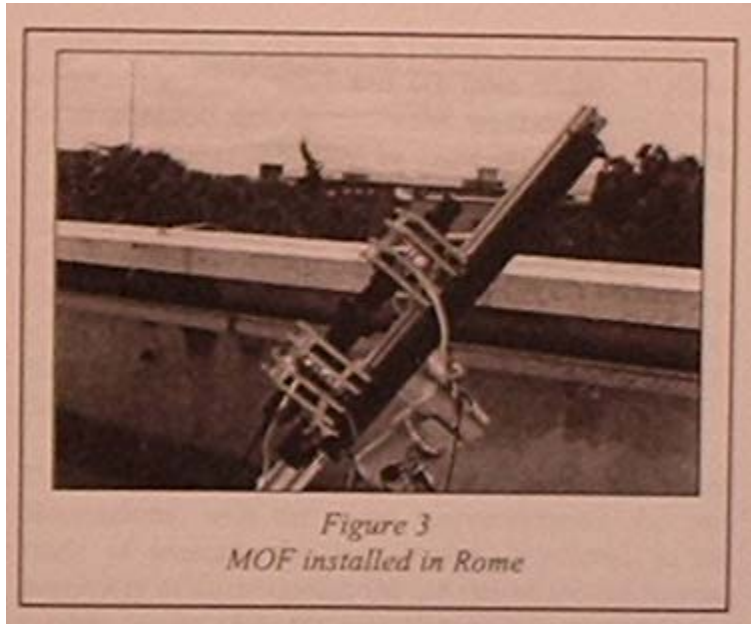**Fig. 1 Mechanical assembly of the instrumentation**

Figure 3
MOF installed in Rome

Fig.2

The MOF weights about 1 Kg and its dimensions (10x10x30 cm^3) are also attractive for space applications. This could be desirable to avoid spurious effects from the Earth atmosphere; However, due to the high costs and other difficulties of space projects (as ,for example, the spacecraft motions) , it is preferable to perform our measurements from the ground, taking advantage of the absolute wavelength reference of the MOF and relay on the well known Sun-Earth relative Doppler Shifts at any time.

As a filter, the MOF will be located between the telescope and the image sensor.

In this manner we are able to reject all the other wavelengths of the solar spectrum, but the wanted line, so that we can definitely say that the MOF produces an artificial night, which is the necessary condition to detect faint signals. Fig 4.shows an image taken with a MOF tuned in the core of the Sodium D lines where an intensity reversal (faint emission) can be observed in a very narrow wavelength interval wherever magnetic field is present in the solar surface. The magnetic field excites the emitting atoms, modifies the line profiles and appear well pronounced in

our MOF image. This effect should be taken in due consideration for precise determination of the line shift.

The signal originated by the GRS amounts to 632m/sec (Doppler equivalent). Fig 5 shows a Doppler image of the Sun where the predominant rotation signal (from the East limb to the West limb) amounts to about 4 Km/sec. We have been able to measure Doppler signals as low as 1 cm/sec by integration over the whole solar disk. Fig. 6 shows a plot of the oscillatory signal due to solar p-modes in the 5 minute band (pick-to-pick amplitudes ~ 1 m/sec , integration time= 30 seconds, telescope aperture = 2 cm ; JPL facility, Pasadena, California). Therefore our instrument has the capability to improve considerably the accuracy beyond the few percent so far achieved. Our first goal is to reach the precision of one part per mil.
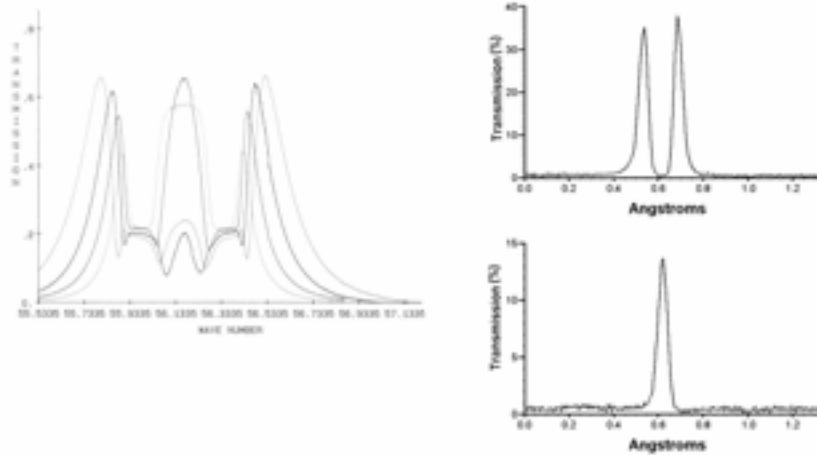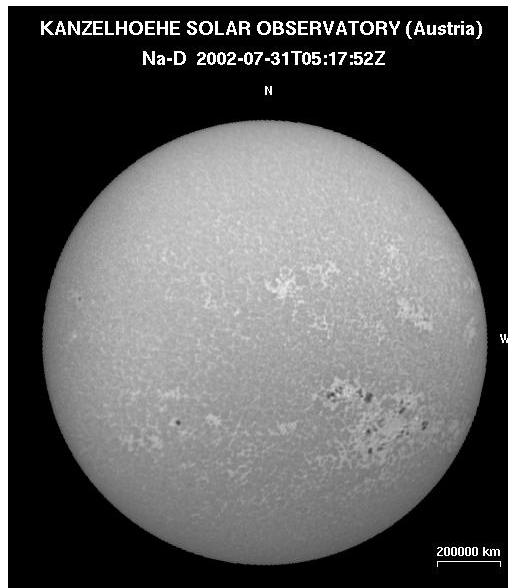

MOF (Transmission Profiles)

Fig.3……………

KANZELHOEHE SOLAR OBSERVATORY (Austria)
Na-D 2002-07-31T05:17:52Z

N

W

200000 km

Fig 1   __MOF, Na I*ntensity image.   Locations of facular regions are well visible and identified.*
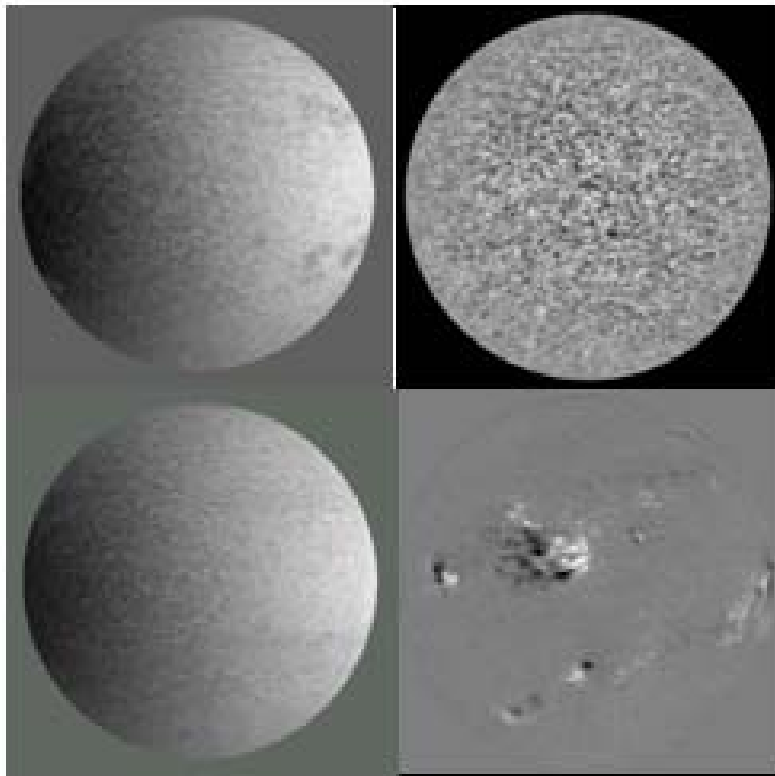

Fig.2— D
Doppler and
Mgnetogram

Fig 4 and 5……………………….

4. The Envisioned Strategy for the Solar GRS Measurement

As stated in the previous section, the MOF is able to measure very small Doppler oscillatory signals. However, the present project deals with a far more difficult problem, that is, the evaluation of a constant additive shift among a number of other known and, perhaps, unknown effects. This is the main challenge of the aimed measurement. We list in the following such effects and how the MOF can help disentangling them.

1-
The sun is gaseous sphere displaying darkening toward the limbs. The GRS is measured looking at the wavelength position of a solar spectral line respect to a laboratory line. This requires a careful study of their intensity profiles (which is a function of position and time) and the availability of high resolution spectrographs. Moreover, also the central wavelength position is a function of time and depends on the point selected on the surface of the Sun. Indeed, the sun is a non homogeneous rotating sphere and its surface displays convective and oscillatory signals amounting to as much as 1 Km/sec (see the mottling in Fig.5). Therefore, a measurement technique that neglects the above local effects, averaging them in a single shot, is definitely not a suitable procedure. A better way of doing would be to measure the wavelength position in all the points at once, in a time interval shorter than the competing signal evolution (possibly few seconds), and proceed to a careful data analysis with the help of the solar Ephemeris and the published data about convection, rotation and center/limb variation of the solar line profile. This cannot be achieved with a spectrograph but only with a Filter, particularly, the Magneto-Optical Filter. See Fig 7
[Few years ago in our laboratory three students have been asked to analize a few images taken with the MOF in Antartica and found that the zero velocity points in a Doppler image can be fitted with a parabola that follows the solar differential rotation in a position that differs from the rotation axis by the right amount of 635 +/- 25 m/sec]

2- The MOF is, by definition, a stable instrument with intrinsic wavelength reference. Therefore, the game is to verify to what extent its stability is maintained during long runs and what is the level of asymmetry between the Red and Blu transmission bands. The Appendix deals with these two problems and we need to check instant by instant their behavior.

3- Different solar lines suffer from different convective disturbances, chromospheric lines, like the Sodium D2, being less affected than photospheric ones, although never free from random-like velocities. An additional chromospheric line, very useful in this context, would be the Calcium resonance @422.7 nm. This is a wide line with a narrow central portion almost entirely chromospheric. In order to take advantage of it, we need to develop a new

MOF for Calcium, as we have proposed since long time ago, but never been able to set up a suitable fabrication laboratory for lack of funds. At the solar limbs, the convective velocities are orthogonal to the line of sight and should become undetectable; on the other end the line profiles undergo modifications, becoming wider and shallower and tangential movements cannot be excluded. For this reason we plan to observe multiple lines simultaneously, the Sodium doublet, the Potassium resonance line @770 nm and, hopefully, the Calcium 422.7. A comparison among their behaviors, all over the solar disk, will help disentangling the convective disturbances or identifying the amount of uncertainty produced by this effect. The scientific literature is full of fine observational works regarding this problem. We can mention here that the Potassium line and the Sodium line are formed at two different levels 300 Km apart (in height) , therefore probing different gravitational potentials: we expect to be able to see such a different effect amounting to about 0.5% of the total effect.

4- The Earth's atmosphere can interfere with the measure adding blends to the pure solar profile. Fig.8 shows the Sodium solar doublet and, separately, the atmospheric lines (mainly H_2O) at the bottom of the figure. Their occurrence and equivalent width is a function of time (hourly and daily) and location (dryness or humidity) of the observing station. In order to monitor this effect we definitely need continuous data acquisition from more than one station, at least three, at different longitudes. We plan to contact and propose agreements with several Observatories around the world that are available to host our instrumentation

In conclusion, our strategy is to avoid working with a single observing station and few shots at discrete times. The aim is to accomplish prolonged observing runs for more than one year in order to demonstrate their long-term consistency by fitting the earth's orbital motion. This will provide a precise calibration signal, beyond the diurnal and oscillatory shifts. Also, we plan to use more than one solar line, from the photosphere to the chromosphere, that will tell us how convection decays with height towards the chromosphere. Finally, it is important to stress that the MOF Doppler imaging capability and its stable and absolute wavelength reference, will allow us to study such effects as the magnetic contamination, the center-to-limb variations and the local oscillatory or convective velocities.

A few years ago we have asked some students to analyze our Potassium Doppler images following a differential procedure. The result was 635 m/sec, very close to the real GRS, but with an estimated error of +/- 26 m/sec. The analysis was performed looking at the constant velocity contours that follow, in average, the differential rotation curves. In particular, the zero velocity points follow a winding path around the local convective velocities (fig.7). After parabolic fitting, the solar rotation axis was also determined and its equatorial distance taken as a measure of the GRS. This procedure is affected by several sources of errors, as the above distance and its ratio to the solar diameter (also affected by an error). The technique based on the isovelocity levels makes it possible to write down a redundant system

of equations linking the rotation, the blue shift , the limb effect on the line shape, the instrumental biases and , of course the GRS.

Fig 8
Spectrum of the Na doublet from the sun.Also many H2O line are sown belongfing to the Earths atmosphere.

Center

B.SCALE)

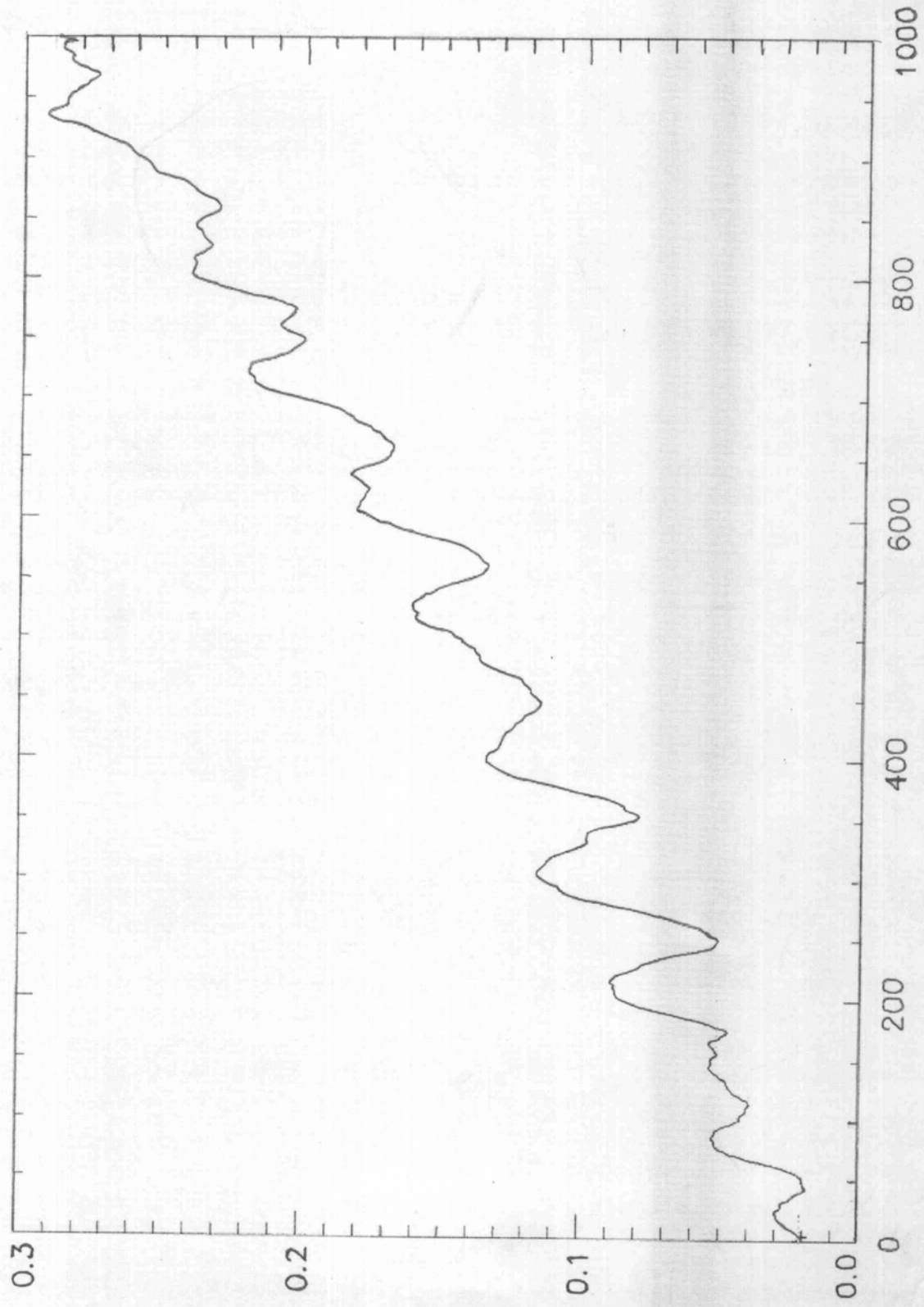Intensity

100   50   0

Wavelength
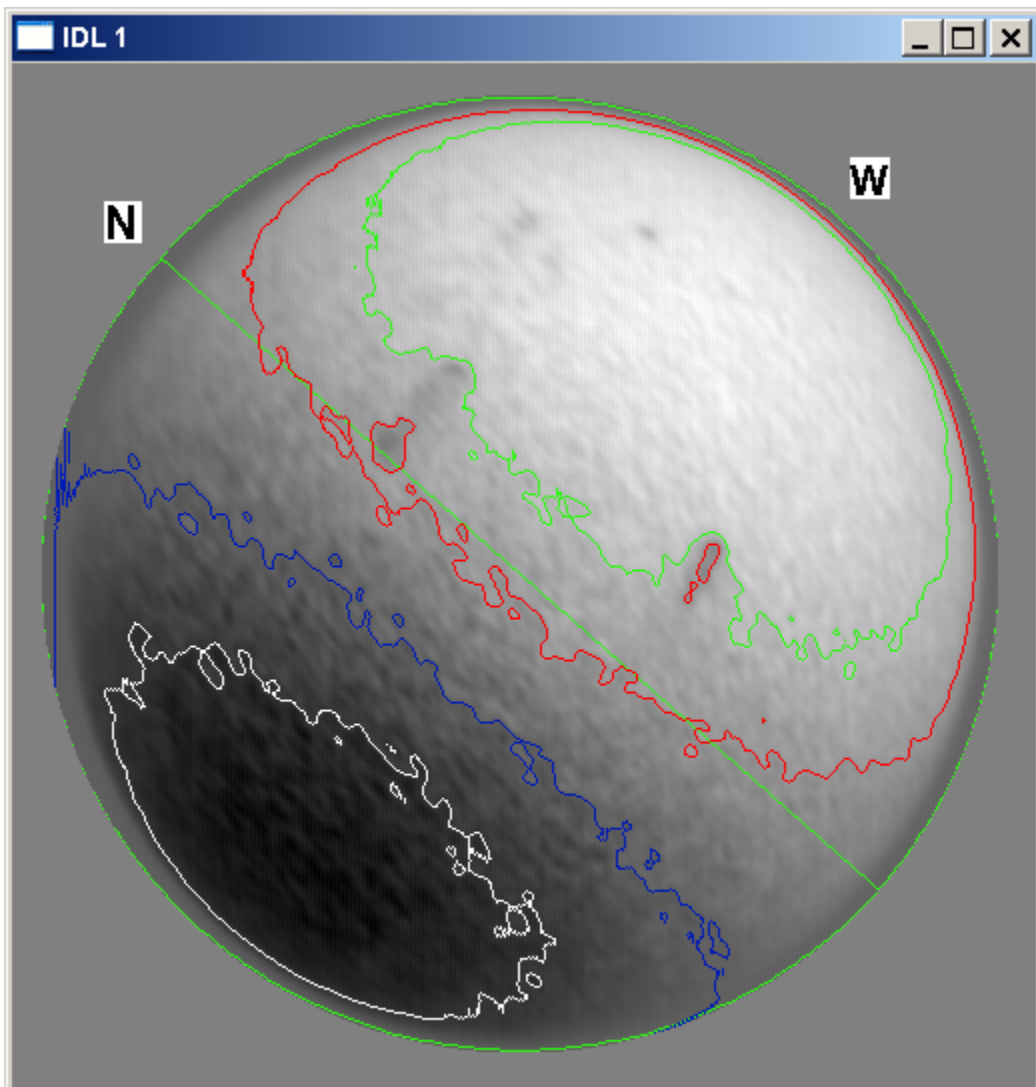
5890

5895

5900
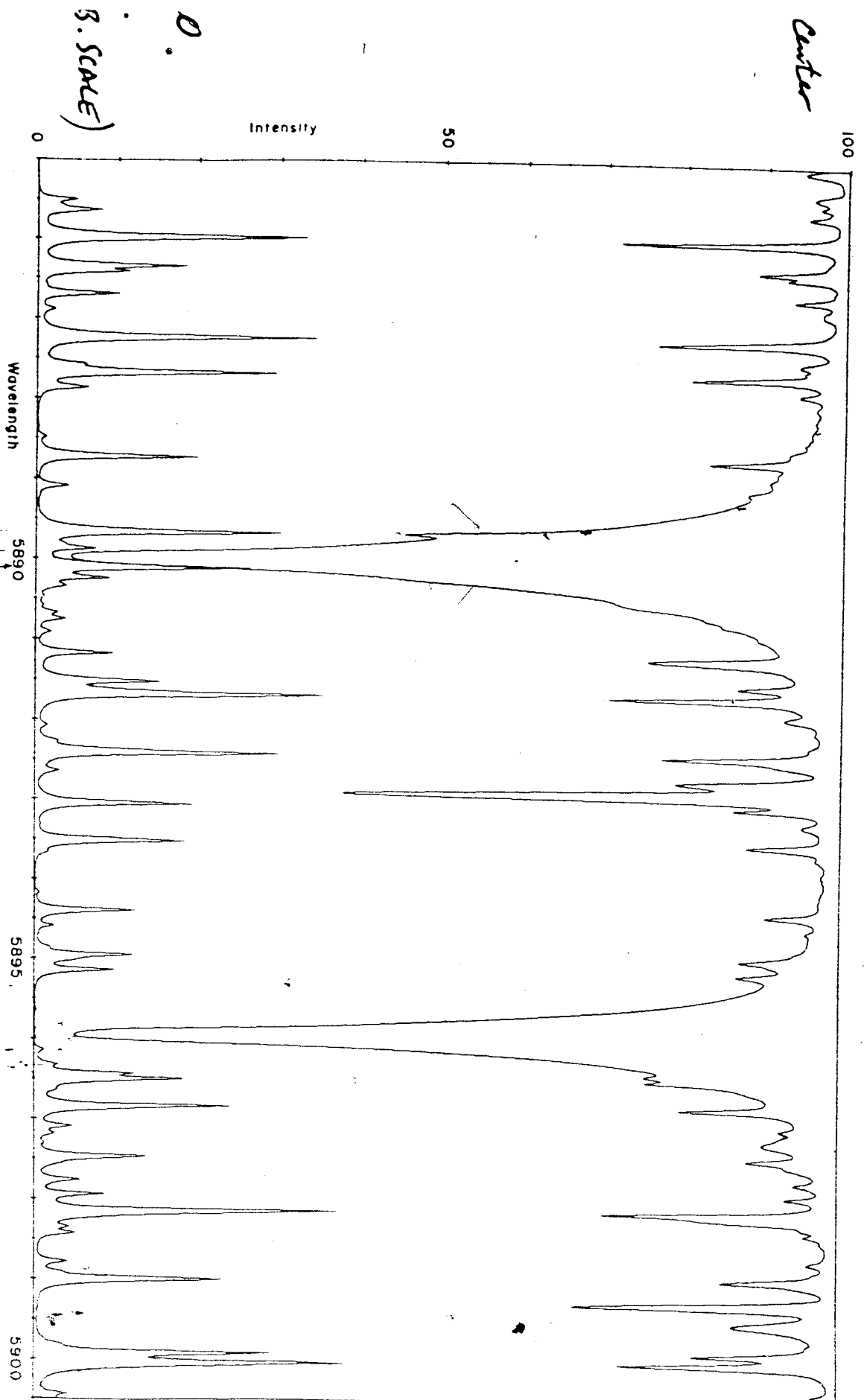
Fig.6

Fig 7 Potassium Doppler image. Four isovelocity levels are shown along with the solar rotation axis. The curvature of the isovelocity curves is originated by the differential rotation that become orthogonal, therefore undetectable, at the polar axis. Nevertheless, the zero velocity level appear as a blue curve whose distance from the solat axis is a first estimate of the Gravitational shift.

The activity will be detailed as follows:
1^ year………………… Instrument fabrication of the clones and visits to the host observatories (signing agreements)
2^ and 3^ years………..Installation , tests and observations
4^ and 5^ years………..Data reduction and additional measurements.

APPENDIX

JPL

THEORETICAL AND EXPERIMENTAL STUDY OF
THE MAGNETO OPTICAL FILTER

A. Cacciani[1]
P. Rosati[1]
D. Ricci[1]
A. Egidi[2]
T. Apporchaux[3]
R.J. Marquedant[4]
E.J. Smith[4]

[1]University of "La Sapienza", Rome, Italy
[2]University of Tor Vergata, Rome, Italy
[3]Space Science Department of ESA, ESTEC, The Netherlands
[4]Jet Propulsion Laboratory, California Institute of Technology, 4800 Oak Grove
Drive, Pasadena, CA 91125

July 1994

PREFACE

This report summarizes work done as a collaboration between JPL and the University of Rome. The work that is reported here was performed over an interval of several years and required the spending of substantial amounts of time at JPL by Alessandro Cacciani, as well as a visit by Donatella Ricci and Piero Rosati. Professor Cacciani spent over two years at the laboratory as a NASA/NRC Senior Resident Research Associate. The six month tenure of Drs. Ricci and Rosati was funded by the Italian Foundation 'Angelo Della Riccia'. The availability of the tunable laser system on which the experimental work is based was funded through the JPL Capital Equipment Fund. The authors express their gratitude to these various sources for their support of this research. Invaluable technical assistance was provided by Jan Van Amersfoort and Lee Wigglesworth. Cacciani acknowledges permission from his home institution, Ministero della Publica Istruzione and Consiglio Nationale delle Ricerche, to spend the required time at JPL.

ABSTRACT

A theoretical and experimental study is reported of the spectral behavior of the Magneto-Optical Filter (MOF). A computer model, capable of reproducing the spectral transmission functions of the MOF, given the values of a few easily measured parameters, has been developed and its results have been successfully compared with high resolution spectral scans obtained at JPL using a tuneable laser. The radiation transfer through the MOF takes into account the temperature and vapour density distribution inside the cell and magnetic field inhomogeneities. The latter involve the computation of the hyperfine structure of the Zeeman pattern at various magnetic field strengths. The model can be used to optimize spectral characteristics of the MOF for diverse applications in solar physics. Use of the MOF as a Doppler analyzer, to detect Doppler velocity shifts of the sodium absorption lines, has been simulated. The sensitivity, linearity and stability of the velocity signal have been investigated. One important result is that the spectral transmission of the MOF is very stable against thermal fluctuations at the level required for helioseismology (approximately 10cm/sec/°C over a range of 3°C).

1. THE INSTRUMENT AND ITS CAPABILITY

The working principle of the MOF has been described, at least partially, in several publications [1,2,3,4,5,6,7]. In what follows, details of its spectral behavior will become clearer. It is essentially a very-narrowband (down to 20 mÅ) and absolutely stable filter (single or multiple pass-band), operating in the center and/or wings of a selected spectral line. It is able to produce monochromatic images of a source emitting in the same lines. Its double pass-band version is being used successfully to obtain doppler and magnetic maps of the sun by computer subtraction of images taken in the red and blue wings of a solar absorption line [8,9].

Before giving the relevant mathematical equations, we discuss the general principles of operation using fig.1. No light is transmitted through two crossed polarizers, P_1 and P_2, unless a depolarizing element, V, is located between them. To achieve a narrow-band transmission, $\Delta\lambda$, V should effect transmission only within $\Delta\lambda$. In our existing MOFs, V is a Sodium or Potassium vapour in a relatively strong magnetic field (several KG). Owing to the induced optical activity associated with the Zeeman effect and related phenomena, the polarization of the incoming beam from P_1 is changed only in and around the Sodium or Potassium absorption lines. Therefore, only these wavelengths can be transmitted through P_2.

In principle, any non-reacting mixture of gases and evaporable elements could be used to make a filter working at several different absorption lines. Non-resonance lines could be considered as well, provided a suitable population of atoms can be produced in the wanted atomic level. Lastly, the Stark effect instead of the Zeeman effect could be used to change the P_1 polarization. So far, for practical reasons and in the interest of simplicity, only the Zeeman effect and resonance lines of easily evaporable alkaline metals have been used.

3

2. PRACTICAL CONSIDERATIONS

There are several practical difficulties to be confronted when fabricating and operating an MOF. In fig. 1, we suppose that perfect polarizers are available. Actually, they are characterized by their extinction ratio, ε, that is, the fraction of light transmitted through two crossed polarizers. ε should be small enough that the transmitted intensity in the wanted $\Delta\lambda$ is greater than the overall transmission in the unwanted wavelengths. That is,

$$\epsilon \int_{\Delta\lambda_{overall}} F(\lambda)d\lambda < \int_{\Delta\lambda_{MOF}} F(\lambda)T(\lambda)d\lambda \tag{2.1}$$

where $F(\lambda)$ is the input spectrum and $T(\lambda)$ is the transmission profile. Thus, ε should be smaller than T average.

For the sun and other stars, F is a blackbody continuum spectrum with superposed absorption lines. Considering equivalent widths of F and T of about 3000Å and 30 mÅ, respectively, ε should be less than 10^{-5}. It may also be necessary to limit the input spectral band using an interference prefilter. A good compromise for Na D lines is a flat-top prefilter of about 30 Å so that both D lines are accepted with little effect introduced by thermal passband drifts.

Care must be taken in order to avoid polarizing stresses in the optical windows of the glass cell containing the metallic vapour, V. Such stresses could effect the overall extinction ratio ε and allow a large amount of continuum light to pass through the crossed polarizers. The best way to avoid this effect is to keep the windows at room temperature and evaporate the metal by heating small reservoirs located in the center of the cell (fig.2). Although this solution introduces certain difficulties related to the vapour confinement inside the glass cell, it has been preferred since the beginning of work with the MOF as producing the best results.

4

The problem of vapour confinement, which is difficult in the cold cell configuration, will be discussed further in the next section. However, to anticipate, the cell is filled with a buffer gas so that an atom dwells a very long time in the center of the cell before migrating to the cold walls where it condenses. In other words, the 'cold cell' solution takes advantage of the diffusion properties of alkaline metals in an inert gas rather than working in the collisionless regime of a highly evacuated 'hot cell' for which it is almost impossible to keep the windows at uniform temperature.

3. THE COLD CELL MODEL

3.1 TEMPERATURE DISTRIBUTION

The first step in the analysis is to evaluate the temperature distribution inside the buffer gas. Neglecting the possible effect of convection, the general equation for thermal conduction at equilibrium is [10]:

$$\nabla \cdot (k \nabla T) = 0 \qquad (3.1)$$

where k, the thermal conductivity, is in general a function of temperature and pressure. To simplify the problem, we assume $k = const$ so that the equation for thermal conduction reduces to the Laplace equation, $\nabla^2 T = 0$, which can be solved given the boundary conditions.

. The boundary conditions (temperatures) are easily measured at a few key points outside the cell: the end windows and the cell-body near them (T_f, see Fig. 2), the neck of the metal containers (T_0) and the heater temperatures (T_{Na}) which we take to be equal to the liquid metal temperature. Other temperatures in the glass walls are fitted assuming an exponential decay. Heat sinks can also be used to change the boundary conditions for optimization of performance. Our computation gives the temperature in a three dimensional mesh with 1 mm distance between points inside the volume of the cell.

5

Fig. 3 shows an isotemperature plot in the central plane, $z = 0$, and a temperature profile along the cell's axis. Note the rapid drop in temperature with distance from the heated reservoirs. In order to improve homogeneity, four reservoirs can be allocated around the cell.

3.2 VAPOUR DENSITY DISTRIBUTION

There are significant differences between designs based on the hot cell and the cold cell mentioned above. In the hot cell, the temperature is considered almost uniform and the vapour density is simply given by the saturation vapour pressure curve as a function of temperature for the given metal. Confinement is assured by the glass walls and condensation is avoided by keeping the windows slightly warmer than other parts of the container. A disadvantage of this method is that it is almost impossible to keep the windows at uniform temperature so that thermal stresses occur and introduce unwanted birifringence between the two crossed polarizers.

In the cold cell method, the temperature is almost at room temperature and uniform everywhere except close to where the metal is being evaporated. The gas dynamics is governed by diffusion and an atom leaving the liquid phase undergoes many collisions inside the buffer gas before reaching the glass walls where it condenses. Atoms in a small volume in proximity of the reservoirs survive a long time and only a small amount of metal needs to be evaporated in order to maintain a suitable density in the vapour state. As the vapour atoms migrate, following paths of density gradient (towards the closest wall of the cell), more metal evaporates keeping the density distribution constant. Eventually, the end windows will be coated, but the rate is so slow that cells can be operated continuously for many months. Furthermore, when coating occurs, it is sufficient to warm the windows up for a few minutes to clean them completely.

6

To compute the vapour density of atoms diffusing in the buffer gas, there are two limiting cases to take into consideration. First, the continuity equation for the flux, J, (J = ρv, where ρ is mass density of sodium and v is the local average particle speed) is assumed to be valid, that is,

$$\nabla \cdot J = 0, \tag{3.2}$$

which means that there are no sources or sinks inside the vapour. In the second case, the continuity equation is assumed not to be valid because atoms and molecules quickly recombine as in the case of saturated vapour. Saturation certainly holds at the boundary layers where both condensation and evaporation occur. The saturation regime is simple to model using the saturation pressure curves once the temperature distribution is given. Comparison of our computations with experimental measurements definitely exclude the possibility that the saturation regime holds inside the vapour cloud. For such a case, computation shows that the optical depth would be a factor of 10^3 less than with the pure diffusion regime and no light would be transmitted by the MOF at the usual working temperatures. In general, the situation is intermediate between pure diffusion and saturation.

Adopting the hypothesis of no sinks or sources (except at the boundary layers), the diffusion equation for the mass flux can be written:

$$J = -D \nabla\rho - D \ (k/T)\nabla T, \tag{3.3}$$

where D is the diffusion coefficient. The term, $-D \nabla \rho$, is the contribution to diffusion driven by the density gradient and $D(k/T)\nabla T$ is that driven by the temperature gradient (thermal diffusion). In what follows, we have actually neglected the thermal diffusion as appropriate to very low densities [10]. The continuity equation for J then becomes

$$\nabla D \cdot \nabla\rho + D\nabla^2\rho = 0. \tag{3.4}$$

7

The density, $\rho(x,y,z)$, can be computed once the temperature distribution and the boundary conditions for ρ are given. At the boundary layers, where condensations and evaporation occur, saturation is assumed, that is, the density is given by the saturation vapour pressure at the local temperature.

Fig. 4 shows computed density profiles (along the axis of the cell and the two principal directions of the central section). For comparison, maps of columnar densities are shown in fig. 5. Better homogeneity of the columnar densities inside the useful aperture can be achieved by heating all four of the reservoirs which are located at 90° from each other. However, two reservoirs at 180° are more than adequate for most applications.

Fig. 2 shows the MOF input parameters used to define the temperature boundary conditions. The model is most sensitive to temperatures T_0 and T_{Na}. These temperatures depend on geometrical factors and thermal contacts and are difficult to estimate. This is, inevitably, a source of uncertainty in the predictions of the model, the heater temperature being the only easily measured parameter.

4. TRANSFER OF POLARIZED RADIATION ALONG THE CELL

Once temperature and density distribution have been evaluated inside the vapour cloud, one has to study the transfer of the polarized radiation through the Filter. The vapour cloud is embedded in a magnetic field generated from an external system (permanent or electromagnets). Fig. 6 shows the measured longitudinal magnetic field on the central axis and off-axis for the MOF in operation at JPL.

We need to integrate the Zeeman effect along the optical path taking into account the spatial profile of the vapour density and of the magnetic field. Here, we present briefly the physics of the transmission mechanism using the analogy of the MOF with a double beam interferometer.

8

Referring to figs. 1 and 7, consider the linear polarization from P_1 as the coherent interference of two beams with opposite circular polarizations. The longitudinal Zeeman effect splits both the absorption coefficient and the refraction index. This produces, respectively, absorption of one of the two beams (Righi effect) and phase retardations between them (Macaluso-Corbino or Faraday effect) in a narrow band with a sharp wavelength dependence. For both reasons, the polarization of the recombined beam is changed and the associated radiation is transmitted through the second polarizer, P_2. Thus, the MOF can be considered a two beam interference device for polarized radiation.

Note that there is no physical beam splitting. Therefore all the critical problems connected with mechanical and thermal stability of a double beam device are avoided. The two oppositely polarized beams, while belonging to the same optical ray, are absorbed and retarded differently at specific wavelengths by the Zeeman effect only. Also, there is no free spectral range and critical angular dependence as in other interferometers.

The mathematical model can be derived simply using the Jones matrix calculus [11]. Fig. 7 gives a description of the MOF physical behavior in terms of a double beam interference device. The input of the MOF is a linear polarization represented by a two component vector, say vertical $(0,1)$, which can be split into two vectors circularly polarized, in left $(-i, 1)_L$, and right $(i, 1)_R$ handed senses.

The two circular vectors interact with the vapour in a magnetic field through the Zeeman effect and finally are recombined through the end polarizer P_2. The effect of the vapour is also describable by the Jones formalism through matrix operators applied sequentially to the polarization vectors. The matrix operator just left of the output vector in fig. 7 represents the phase retardation δ and includes the absorption factor $e^{-\tau}$. The succeeding matrix operator represents the effect of the exit

9

polarizer at $90°$. The final transmitted intensity, that is the squared modulus of the sum of the two resulting vectors, is

$$T(\lambda) = \frac{1}{8}(e^{-\tau^+} - e^{-\tau^-})^2 + \frac{1}{2}e^{-(\tau^+ + \tau^-)}\sin^2\frac{\delta}{2} \quad .$$

δ and τ are functions of wavelength and are given by the Zeeman pattern for the left and respectively right cirular components (σ^+, σ^-). They result from integration along the optical path z where vapour density and magnetic field are functions of position:

$$\tau_\lambda^\pm = \int_0^\ell \left(\frac{d\tau_\lambda^\pm}{dz}\right) dz$$

$$\delta_\lambda = \varphi^+ - \varphi^- = \int_0^\ell \left(\frac{d\varphi_\lambda^+}{dz}\right) dz - \int_0^\ell \left(\frac{d\varphi_\lambda^-}{dz}\right) dz$$

with

$$\left(\frac{d\tau_\lambda}{dz}\right)^\pm = \sum_i \left(\frac{d\tau_\lambda}{dz}\right)_i^\pm = \left(\frac{d\tau_0}{dz}\right)\sum_i \left(\frac{f_i}{f}\right)^\pm \frac{H(a,y_i^\pm)}{H(a,0)}$$

$$\left(\frac{d\varphi_\lambda}{dz}\right)^\pm = \sum_i \left(\frac{d\varphi_\lambda}{dz}\right)_i^\pm = 2\left(\frac{d\tau_0}{dz}\right)\sum_i \left(\frac{f_i}{f}\right)^\pm \frac{R(a,y_i^\pm)}{H(a,0)}$$

where

$$\left(\frac{d\tau_0}{dz}\right) = \frac{\sqrt{\pi}}{2}\left(\frac{e^2}{mc^2}\right) f\rho(z)\frac{\lambda_0^2}{\Delta\lambda_D}H(a,0)$$

$$a = \frac{\Delta\lambda_\gamma}{\Delta\lambda_D} \quad \text{(natural-Doppler width ratio)}$$

$$y_i^\pm = \frac{\lambda - \lambda_{0_i}^\pm}{\Delta\lambda_D} \quad .$$

$\lambda_{0_i}^\pm$ are the wavelength positions of $\sigma^\pm$ Zeeman components; f is the oscillator strength of the D lines. To is the optical depth at the central wavelength λ_0 of the line. In addition, $\Delta\lambda_\gamma = \frac{\gamma}{c}\lambda^2$ and $\gamma = \gamma$ (natural) $+ \gamma$ (collisional) $= 1.18 \times 10^{-4}$ Å (from Heitler [17]). The relative intensities (fi/f) of the Zeeman components fulfill Σ_i (fi/f) $= 1$, where the summation is over all hyperfine components. $H(a,y)$ and $R(a,y)$ are the well known Hjerting and Rachkowsky line

10

$$\alpha_i(\Delta E) = \sum_{j=1}^{N} \alpha_j \mathcal{H}_{ij} , \qquad i = 1, \ldots, N \tag{5.2}$$

where $\mathcal{H}_{ij} = \langle \psi_i^{(0)} | \mathcal{H} | \psi_j^{(0)} \rangle$ are the hamiltonian matrix elements in the basis of the known degenerate wavefunctions and the i or j index represents a quantum numbers pair (m_I, m_J) related to which the degeneracy holds.

The eigenvalues ΔE_i yield the energy levels L_i, from which the splittings of the D_1 and D_2 lines can be obtained. The eigenvectors $\alpha^{(L_i)} = (\alpha_1^{(L_i)}, \ldots, \alpha_N^{(L_i)})$, corresponding to the eigenvalue of the level L_i, yield the coefficients allowing the generic wave function ψ_{L_i} to be expressed as a linear superposition of the basis wave functions, that is

$$\psi_{L_i} = \sum_{k=1}^{N} \alpha_k^{(L_i)} \psi_k^{(0)} \tag{5.3}$$

Then, relative line intensities are calculated from the squares of the transition electric-dipole moment matrix elements between a pair of states written above (5.3):

$$D_{L_i, L_j} = \langle \psi_{L_i} | \hat{r} | \psi_{L_j} \rangle = \sum_{k, k'=1}^{N} \alpha_k^{(L_i)} \alpha_{k'}^{(L_j)} d_{k, k'} \tag{5.4}$$

where the (5.3) has been used and the reduced electric-dipole moment elements between unperturbed levels have been defined as

$$d_{k, k'} = \langle \psi_k^{(0)} | \hat{r} | \psi_{k'}^{(0)} \rangle$$

For the energy levels leading to the Na-D_1 line ($^2S_{1/2}$ and $^2P_{1/2}$) an analitical solution given by Breit and Rabi also exists [15]. On the other end, for the D_2 transition, involving $^2S_{1/2}$ and $^2P_{3/2}$ levels, a numerical diagonalization had to be done.

The many hyperfine components have a complicate behaviour for low magnetic field and start becoming symmetric only for field strength larger than 1500 gauss. At about 3000 gauss I and J reach a complete decoupling (Back-Goudsmith effect, or Paschen-Back effect for hyperfine structure). This behaviour combined with the

1 2

range of magnetic field and vapour density inside the cell, produces an asymmetric transmission profile for low magnetic fields as shown in the next section. The magnetic field normally used in solar measurements range from 1.5 to 3.5 kgauss inside the region where most of the vapour occurs (compare figs. 4 and 6). In this case the strong magnetic field approximation gives fairly good results. A scheme summarizing the theoretical model of the MOF is given in fig. 9.

6. EXPERIMENTAL STUDY OF A TWO SODIUM CELL MOF

Previous models of the MOF have not been thoroughly tested because a study of the spectral behavior of the MOF at high spectral resolution was not available. In this report, we present for the first time the spectral transmission of a sodium MOF measured at JPL using a tunable dye laser having a spectral bandwidth less that 5 MHz (0.057 mÅ), which is to say, a spectral resolution much greater than the spectral variations of the MOF itself.

A block diagram of MOF spectral transmission measurements is shown in fig. 10. The reader is referred to ref. [16] for further details.

Spectral transmission of the Filter Section and Wing Selector (see next section) have been measured for combinations of longitudinal magnetic fields between 1.0 and 3.0 KG and sodium reservoir temperatures between 240° and 270° C. The family of spectral transmission curves as a function of these two parameters allows one to verify the overall model described above. Thus, a basis is provided for estimating the MOF's spectral parameters given the value of easily measured parameters, which is what one requires for solar physics and other applications.

As mentioned above, the two input parameters, T_0 and T_{Na}, are difficult to evaluate. Thus, we have elected to use T_0 as a free parameter in order to match the theoretical curves with the experimental ones. This degree of freedom is also useful in compensating for

13

certain approximations introduced into the theory (thermal diffusion and molecular recombination have been neglected and an idealized geometry has been adopted).

A satisfactory agreement between theoretical and experimental curves has been reached by adjusting T_0 in small steps from T_{Na}. However, uncertainties still remain due to the lack of an exact knowledge of the magnetic field throughout the cell. In fact, magnetic field configurations have been confined to the longitudinal case only and transverse field leakages were not investigated. Spectral variations could occur for different cells at a measured fixed temperature because of changes in the amount of sodium in the cells' reservoirs and in thermal contacts when measuring the temperature. In such a case a temperature shift of the input parameter T_0 would be required to recover the observed spectral behavior.

Fig. 11 a,b show a family of measured and calculated curves at a constant magnetic field of 1.5 KG and variable temperature for D_1 and D_2 lines. Fig. 12 shows curves at a constant temperature of 240°C and a variable magnetic field for the D_1 line. The theoretical curves have been calculated for a single light path along the central axis of the cell in order to minimize the computing time. This accounts for their irregular behavior around the Zeeman plateaus and for systematic differences in the amplitude of the transmission peaks. By averaging along different off-axis light paths, in order to fit the 0.8 cm diameter laser beam used in the experiment, one obtains a better agreement. In fact, the contribution of the off-axis light paths, characterized by different magnetic field profiles and, most importantly, optical depths, smooths out the irregularities and lowers the transmission peaks. An example is shown in fig. 13. In this case, calculations show that differences between measured and calculated spectral transmission curves never exceed 10 percent for temperatures from 240 up to 270°C and magnetic fields from 1.0 up to 3.0 KG.

Figure 12 can be used to study the effect of changing field strength on the separation of the lateral peaks, although optical depth is a more important parameter. Such an analysis shows the separation is proportional to $B^{0.6}$. In contrast, Appourchaux (1987)

14

demonstrates a theoretical dependence of $B^{0.5}$ based, however, on an asymptotic expression for the Zeeman splitting in the high field regime.

Apart from these minor differences, the dynamical spectral behavior of the MOF as a function of T and H is well reproduced by the model as shown in Table 1 which compares the calculated and measured spectral sensitivities of the filter peaks with respect to magnetic field and temperature. This agreement enables us to find the best tuning of the spectral parameters of an MOF of the type used to study solar oscillations and solar magnetic fields.

7. OPTIMIZATION OF SPECTRAL CHARACTERISTICS FOR APPLICATIONS IN SOLAR PHYSICS

The MOF used in solar physics is comprised of two sections. The first section, called the Filter, described above (fig.1), generates two transmission bands. The second section, called the Wing Selector, consisting of a $\lambda/4$ plate and a second cell immersed in a longitudinal magnetic field, absorbs one band while transmitting the other [8,9]. Using an electro-optical light modulator, the red and the blue wing of the solar sodium absorption line can be alternately sampled. Spatially resolved images or integrated disk measurements of the Sun are obtained in both positions, thereby , the Doppler shift or Zeeman splitting of the solar line relative to the central wavelength can be deduced by the difference of intensity in the two wings after proper normalization.

The peak absorption wavelength of the Wing Selector depends on the Wing Selector's magnetic field, the temperature affecting only its bandwidth. In order that one wing of the Filter section be blocked, one has to use a magnetic field at least 1.5 KGauss stronger than the field in the Filter section, the goodness of matching depending on the temperature of the Filter.

The magnetic field and temperature of the two MOF sections (H_F, H_{WS}, T_F, T_{WS}) have to be suitably tuned in order to optimize the spectral characteristics, i.e., to obtain narrow

1 5

optical bandwidth, little out-of-band leakage and high transmission. In fig.14a, optimized MOF transmission profiles are shown, as obtained from experimental data, together with the sodium solar absorption lines. The vertical transmission scale includes transmission losses due to the calcite polarizers and the windows of the sodium cells. Fig. 14b shows the corresponding calculated curves. By convolving MOF theoretical profiles with the solar absorption lines, the velocity signal can be evaluated. Thereby, the sensitivity and linearity of the response with respect to the Doppler velocity can be studied.

The measured response of the MOF over an extended range of velocities is presented in Figure 15a. The signal, as shown, is derived from intensity measurements (I_R, I_B) in the red and blue wings of the sodium absorption line. The data were obtained by using the MOF to make global solar measurements. A heliostat, retrieved from another JPL project, was added to the JPL magnetics laboratory, Bldg. 253 (where the tuneable filter was also housed). The solar image was relayed to a work bench inside the building on which the MOF, a lock-in amplifier, a strip chart recorder, and other peripheral equipment were co-located. Measurements could be made over an entire day so that a large range of radial velocities could be covered. The differential velocities were associated with the rotation of the Earth and its slightly elliptical orbit about the sun. The data were obtained as a function of local time. The latter was then converted using the following equation:

$$v(t) = v_0(t) + v_G + v_r \sin{[\pi(t-t_0)/12]}, \qquad (7.1)$$

where the radial component of Earth's orbital velocity is $v_0(t)$, the gravitational red shift, $v_G = 636$ m/s, the rotational velocity of the Earth is $v_r = \Omega_E r_E \cos(L) \cos(\Delta)$, with $r_E =$ Earth radius, $\Omega_E =$ Earth rotation rate referred to the sun (solar day), $L =$ geolatitude of observing station, $\Delta =$ declination of the sun and t_0 is local time referred to noon, i.e., $t_0 = 12$ hr.

Although Figure 15a was used primarily to determine the sensitivity of the MOF, the data reveal an offset or bias such that the signal is not zero at zero velocity. This bias could

1 6

be caused by asymmetric transmission of the filter, stray polarization and/or other unknown causes related to the observing procedures and analysis.

The sensitivity of the MOF as a function of filter temperature as derived from calculations based on the model is shown in Figure 15b. The sensitivity, $\delta s/\delta v$, was obtained by calculating the signal as a function of velocity over the range of $\pm 2km/sec$ (the extremes of the radial component of the sun's rotational velocity at the limbs) for different value of T_F. The other parameters correspond to those in Figure 14a,b. A straight line was then fitted to the signal whose slope was $\delta s/\delta v$.

One of the main requirements of a Doppler analyzer is spectral stability. Since the MOF has an absolute wavelength reference, it is intrinsically stable. Nevertheless, the transmission function of the Filter section is sensitive to thermal fluctuations through changes in amplitude and in the wavelength position of the Macaluso-Corbino transmission peaks. On the other hand, the Wing Selector is only slightly sensitive to temperature changes, the peak absorption wavelengths being determined by the Zeeman effect. However, these fluctuations in the frequency position and amplitude of the Filter transmission peaks are mainly symmetrical for high magnetic field with respect to the central wavelength, so that only second order fluctuations in the velocity signal will be induced. Taking constant T_{WS} and varying T_F one expects that a maximum of the signal will be reached at a temperature such that the Filter's bandpasses matches the Wing Selector's wavelengths.

The thermal behavior of the MOF has been experimentally investigated using the integrated solar disk oscillation facility at JPL. By evaluating the instrument response to temperature perturbations, it turns out, both experimentally and theoretically, that the MOF can be tuned so that thermal fluctuations of the velocity signal do not exceed 10 cm/s/°C in a 3°C range around a suitable working temperature. This implies that the noise velocity signal due to thermal fluctuations is ~ 1cm/s at the level of the experimental thermal stability (±0.1°C).

17

8.0 CONCLUSION

The theoretical model described above (see fig. 9) is able to predict the spectral transmission function of the MOF including the fine details evident in the high resolution spectral study carried out at JPL. Inevitable simplifications when evaluating the fluid dynamical behaviour of sodium vapours and departures from a simple longitudinal magnetic field scheme could account for the remaining slight differences. The model suggests how to choose the magnetic field and temperature of the two MOF sections in order that optical bandwidth, spectral purity and transmission may be optimized. Such spectral characteristics determine the sensitivity, linearity and stability of the MOF operating as a Doppler analyzer. A simulation of an experiment to measure low degree solar oscillations, which is now being carried out at JPL, also suggests suitable parameter settings in order to meet the instrumental requirements of helioseismology. An MOF can be configured having high sensitivity and stability and a linear response over an adequate dynamic range. Specifically, the stability of the MOF against thermal fluctuations which is the major source of noise in the velocity signal, has been shown to be suitable for the detection of velocity signals with amplitudes as small as 1 cm/s.

9.0 REFERENCES

1. Cacciani, A., 1967, *Atti. Soc. Astr. Journal, Italiana.*

2. Cacciani, A., Cimino, M., Sopranzi, N., 1966, *Bull. Soc. Ital. Fis.*, 50 Commun. 4.B.8.

3. Cimino, M., Cacciani, A., Fofi, M., 1970, *Solar Phys.*, 11, 319.

4. Agnelli, G., Cacciani, A., Fofi, M., 1975, *Solar Phys.*, 44, 509.

5. Cacciani, A., Fofi, M., 1978, *Solar Phys.*, 59, 179.

6. Tomczyk, S., 1988, Ph.D. Dissertation, UCLA.

7. Appourchaux, T., 1987, *Solar Physics*, 109, 393.

8. Cacciani, A., Rhodes, E., 1984, *Solar Seismology from Space, The Magneto-Optical Filter, Working Principles, and Recent Progress*, p. 115.

9. Rhodes, E., et al., 1984, Evaluation of a Magneto-Optical Filter and a Fabry-Perot Interferometer for the Measurement of Solar Velocity Fields from Space, Solar Seismology from Space, JPL Publication 84-84, p.125.

10. Lifshitz & Pitaevskii, 1981, *Physical Kinetics*, Pergamon Press.

11. Shurcliff, W.A., 1962, *Polarized Light*, Harvard Univ. Press, Cambridge, Mass.

12. Aller, L.H., 1963, *The Atmospheres of the Sun and Stars*, The Ronald Press Co., N.Y.

13. Beckers, J.M., 1969, *Solar Phys.*, 9, 372.

14. Arimondo, E., Inguscio, M., Violino, P., 1977, *Rev. of Mod. Phys.*, 49(1), 31.

15. Breit, G., Rabi, I., 1931, *Phys. Rev.*, 38, 2082.

16. Marquedant, R.J., Cacciani, A., Smith, E.J., VanAmersfoort, J., Wigglesworth, L., "Experimental Study of a Sodium Vapor Magneto-Optical Filter", Report JPLSP#185, Jet Propulsion Laboratory, Pasadena, California, 1989.

17. Heitler, W., 1960, *The Quantum Theory of Radiation*, Oxford at the Clarendon Press. London.

19

$\frac{\partial \lambda}{\partial H}$ (mÅ/KG)	Theoretical values	Experimental values
D_1	43 ÷ 55	44 ÷ 61
(T = 240 → 270 °C)		
D_2	54 ÷ 71	52 ÷ 81
$\frac{\partial \lambda}{\partial T}$ (mÅ/°C)		
D_1	1.2 ÷ 1.9	1.2 ÷ 2.1
(H = 1.0 → 3.0 KG)		
D_2	1.6 ÷ 2.7	1.8 ÷ 3.4

Tab.1 Peak separation wavelength sensitivity to magnetic field and temperature variation. The measurement error is estimated to be ± 1 mÅ and ± 0.1 mÅ, respectively.
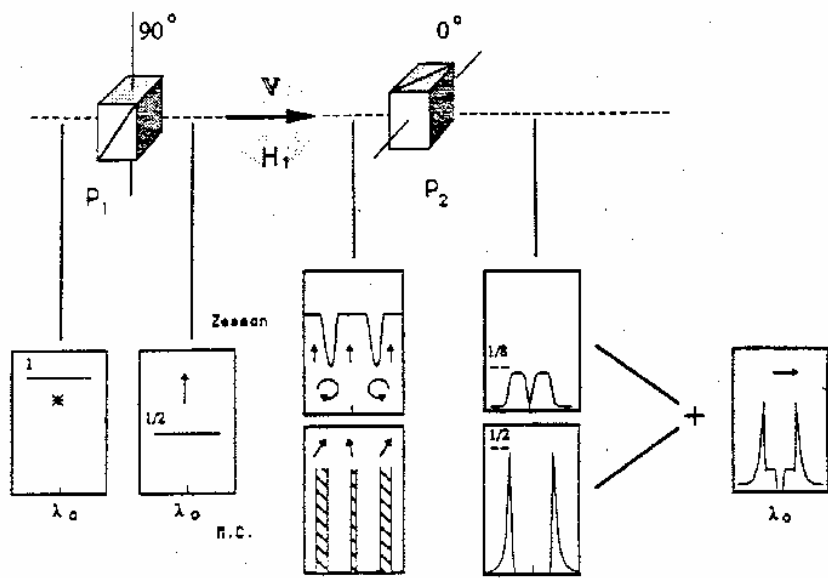
Fig.1   M.O.F. layout and its working principle. Depolarizing effects due to Zeeman and Macaluso Corbino effect are indicated.

21
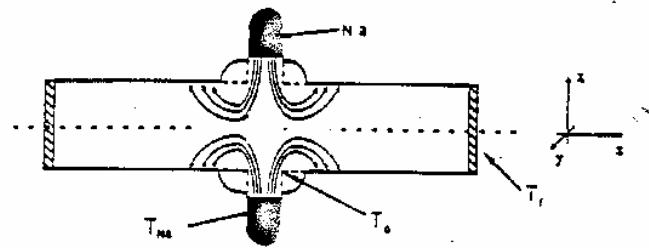
Fig. 2 Sketch of a sodium cell. The temperature parameters T Na, To, Tf are used as input boundary confitions for the model. By diffusion the vapour cloud follows paths as indicated inside the cell.
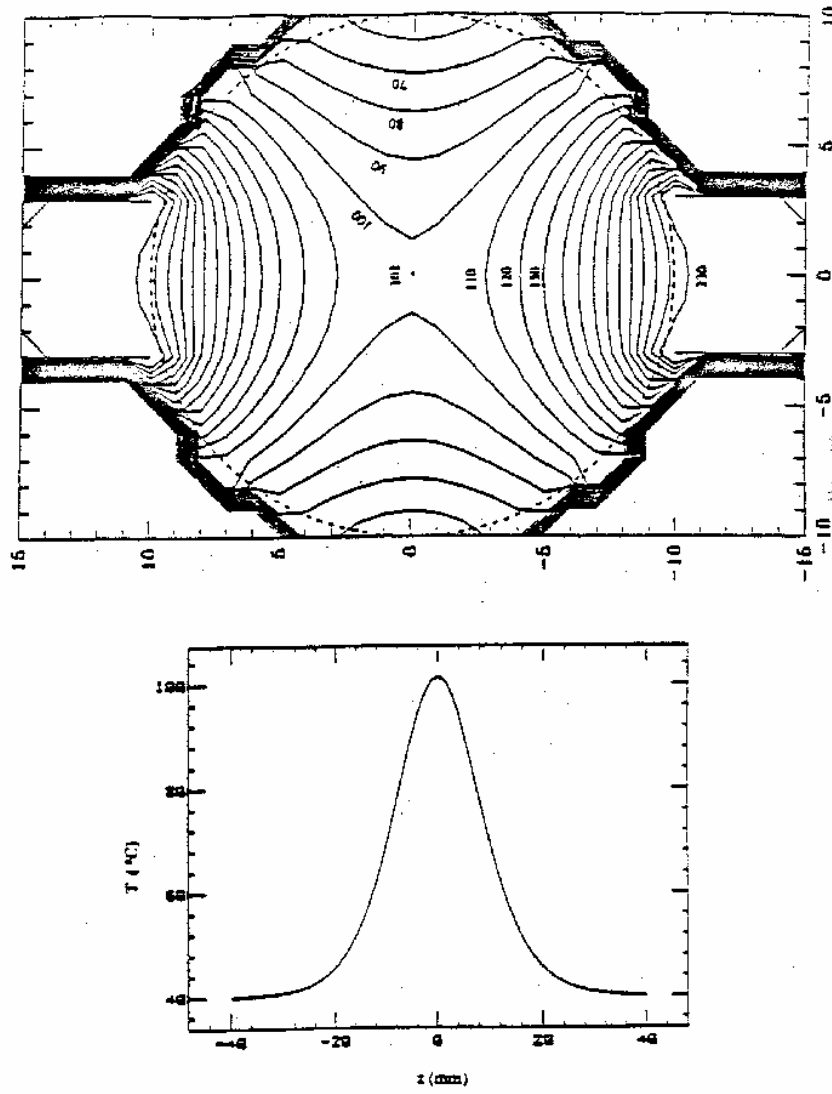
Fig. 3   a) temperature contour plot in the central plane z=0
          b) temperature profile along the cell's axis: $(T_{Na} = T_0 = 250°C)$.
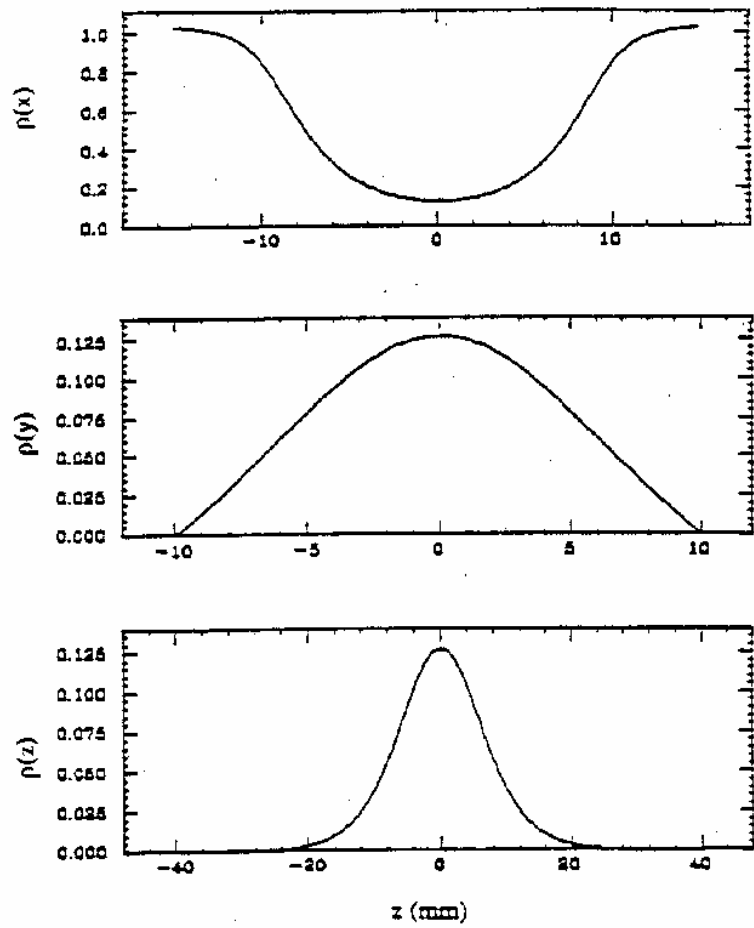
23

Fig. 4 Density (ng/cm^3) profiles along the three axes of the cell corresponding to the temperature setup of Fig.3.

24

Fig. 4 Density (ng/cm^3) profiles along the three axes of the cell corresponding to the temperature setup of Fig.3.

24
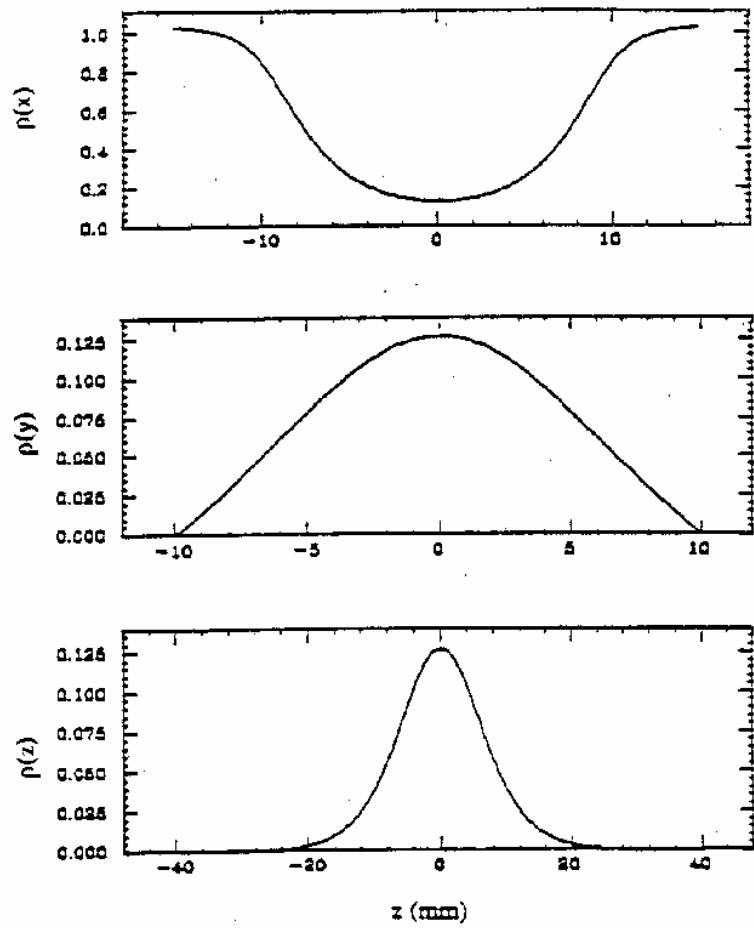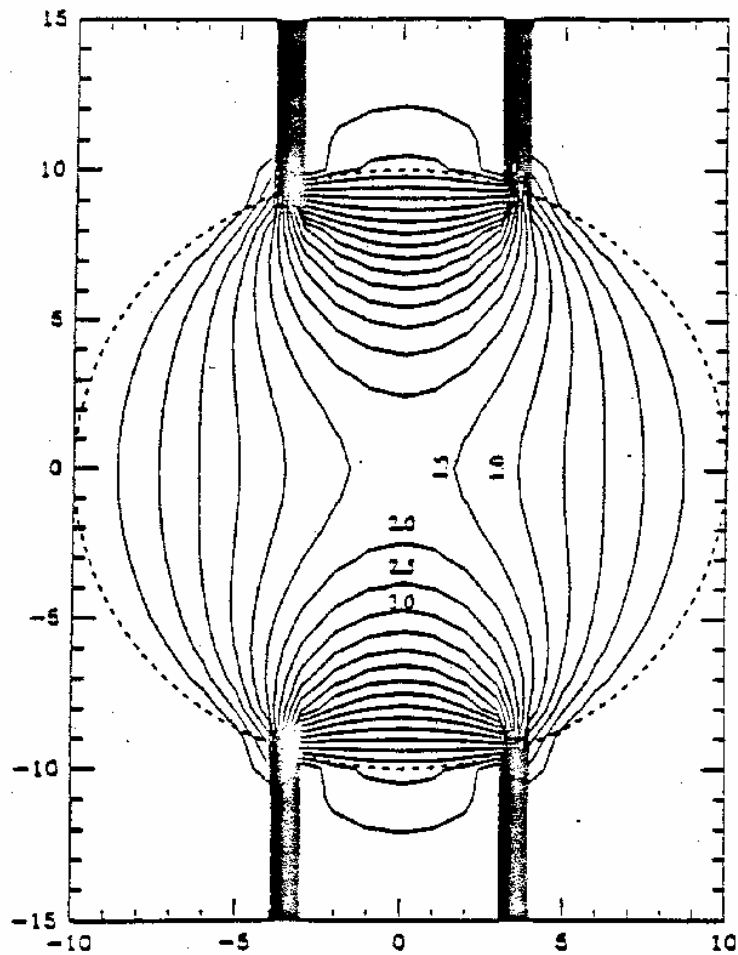
Fig. 5 Map of columnar densities (ng/cm3) along the z axis.

25
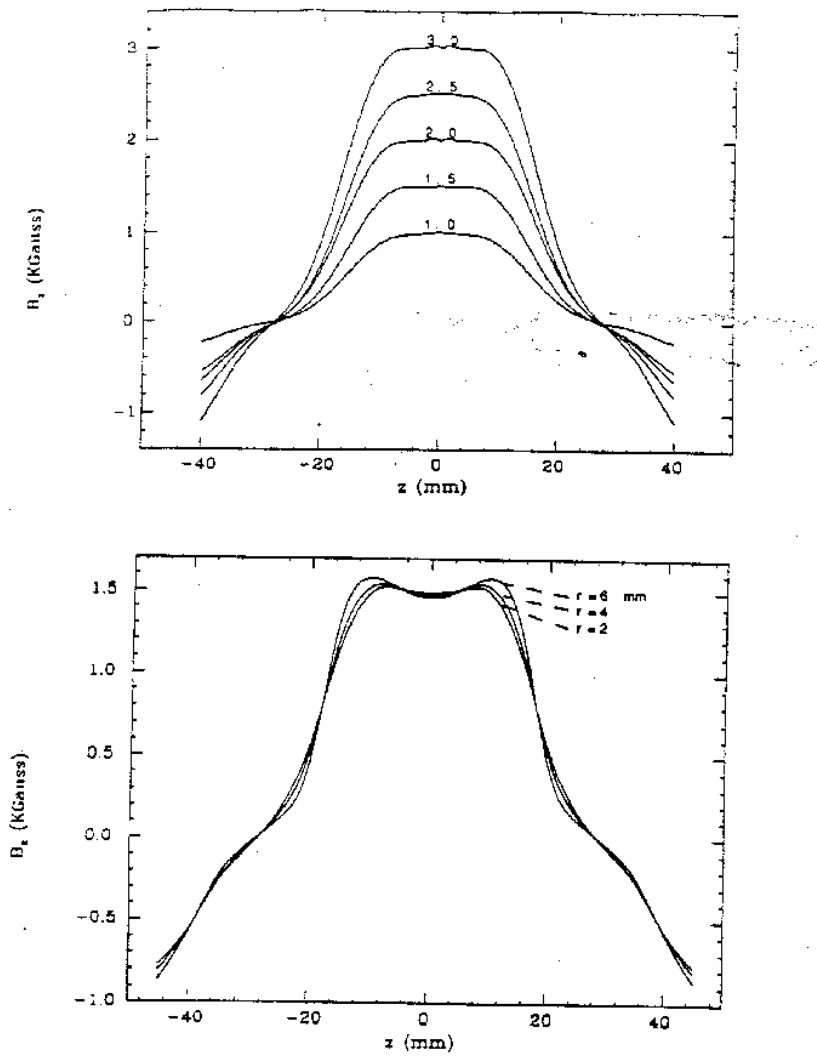
Fig.6   above: measured magnetic field on the cell center line.
        below: measured magnetic field at different distances r off axis ($H = 1.5$ KG).

$$\nu_{IN} = \begin{pmatrix} 0 \\ 1 \end{pmatrix}_I = \begin{cases} \begin{pmatrix} i \\ 1 \end{pmatrix}_R \rightsquigarrow \begin{pmatrix} GAS \\ \beta \end{pmatrix} \rightsquigarrow P_1 \Leftrightarrow \begin{pmatrix} 1 & 0 \\ 0 & 0 \end{pmatrix}_{P_R} \left[\left(\begin{pmatrix} +\cos\delta/2 & \sin\delta/2 \\ -\sin\delta/2 & \cos\delta/2 \end{pmatrix} e^{-\tau} \right)_{OAS} \begin{pmatrix} i \\ 1 \end{pmatrix} \right]_R \\[4ex] \begin{pmatrix} -i \\ 1 \end{pmatrix}_L \rightsquigarrow \begin{pmatrix} GAS \\ \beta_L \end{pmatrix} \rightsquigarrow P_1 \Leftrightarrow \begin{pmatrix} 1 & 0 \\ 0 & 0 \end{pmatrix}_{P_L} \left[\left(\begin{pmatrix} +\cos\delta/2 & \sin\delta/2 \\ -\sin\delta/2 & \cos\delta/2 \end{pmatrix} e^{-\tau} \right)_{OAS} \begin{pmatrix} -i \\ 1 \end{pmatrix} \right]_L \end{cases}$$

$$\longrightarrow \nu_F = T_F(\lambda)$$
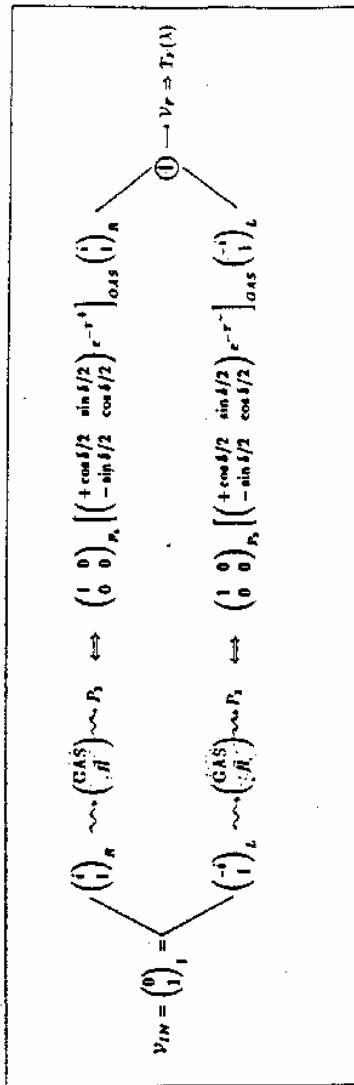
Fig. 7 The MOF as an interferometric device. The amplitudes are disregarded for simplicity.

27
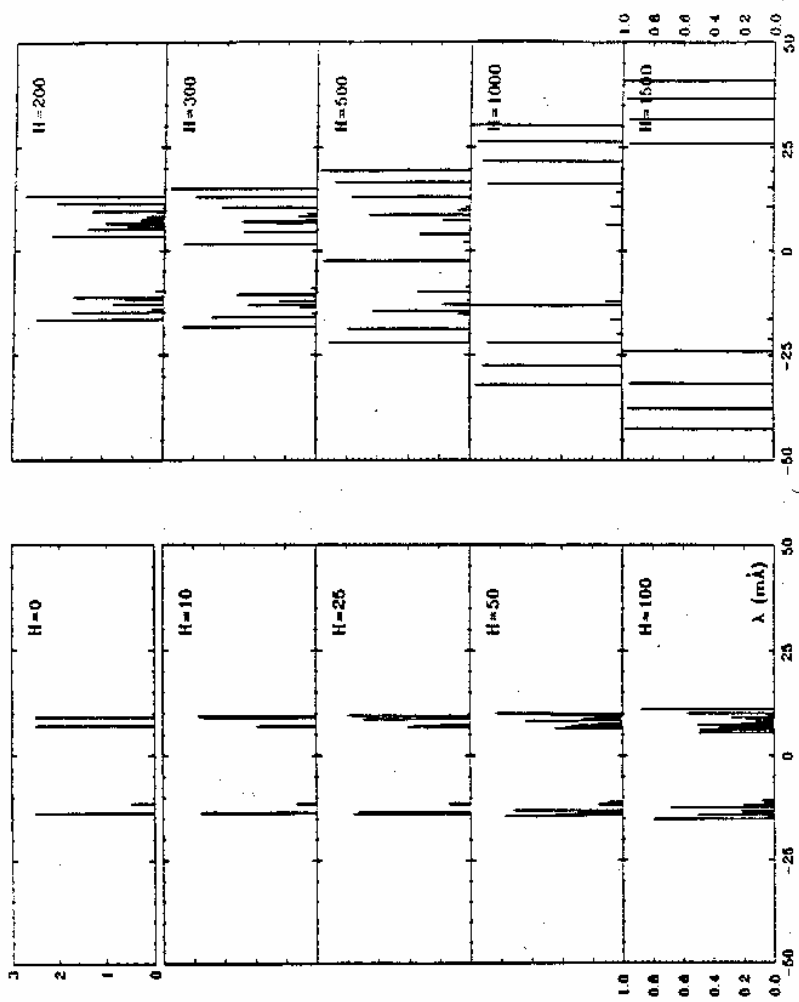
Fig. 8a Hyperfine components of the $D_1\sigma^{\pm}$ sodium lines as a function of the magnetic field.

28
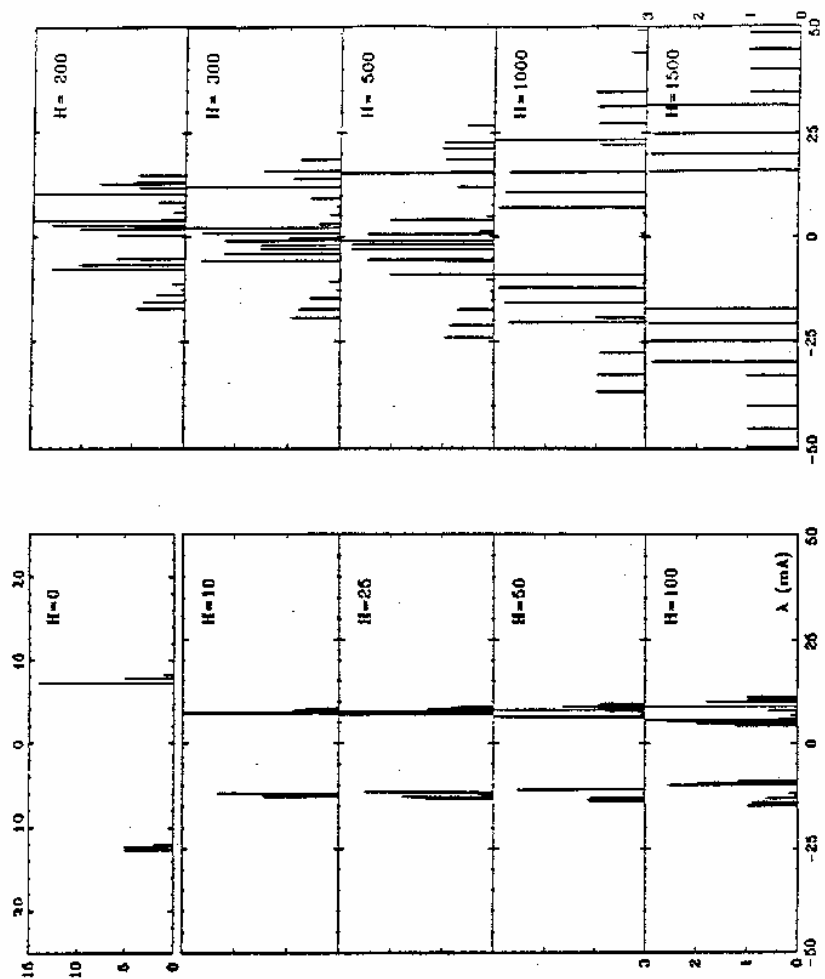
Fig.8b Hyperfine components of the $D_2 \sigma^*$ sodium lines as a function of the magnetic field.

29
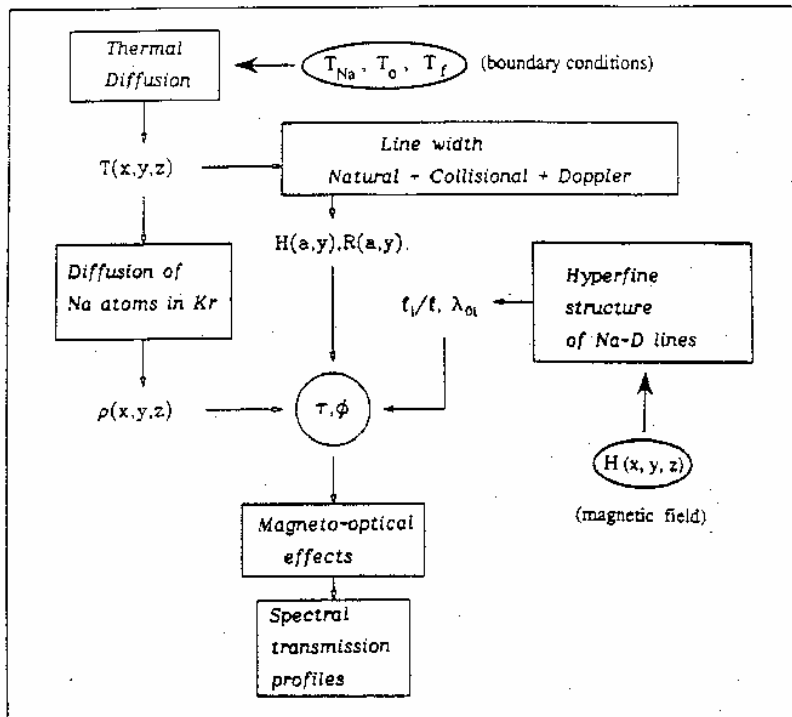
Fig.9　Block Diagram of the MOF's theoretical model. The input parameters are contained in ellipses.
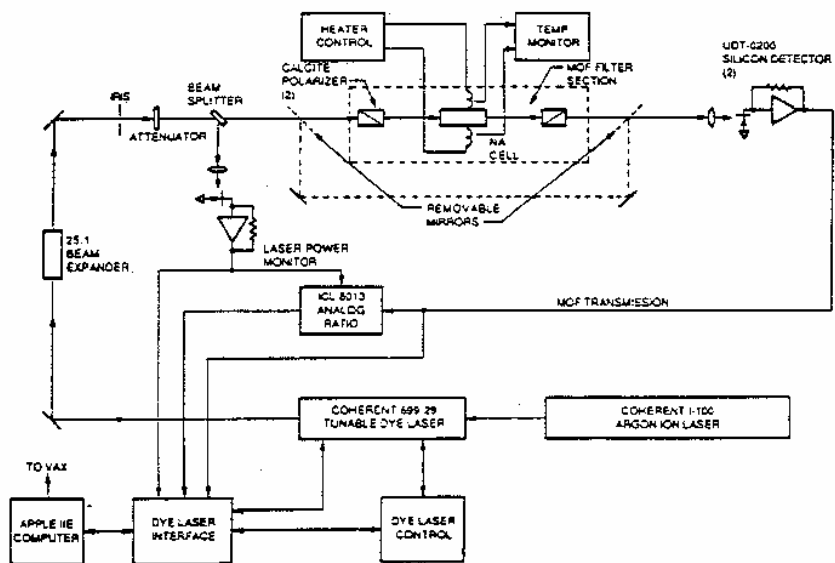
Fig.10 Block Diagram of MOF Spectral Transmission Measurements.
Measurements were made of the Filter section only.

31
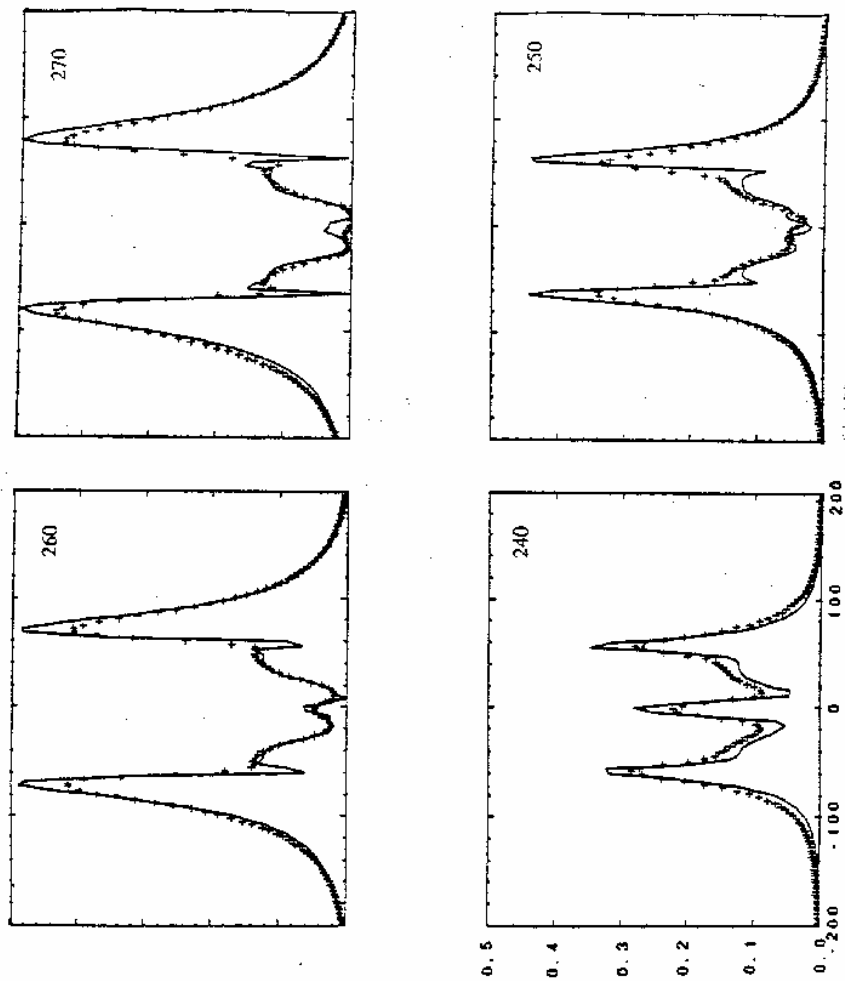
Fig. 11a Calculated and measured (crosses) transmission functions of the MOF for the D_1 sodium line. The x axes show the wavelength in mÅ. H = 1.5 K gauss and T varies from 240 to 270° C.
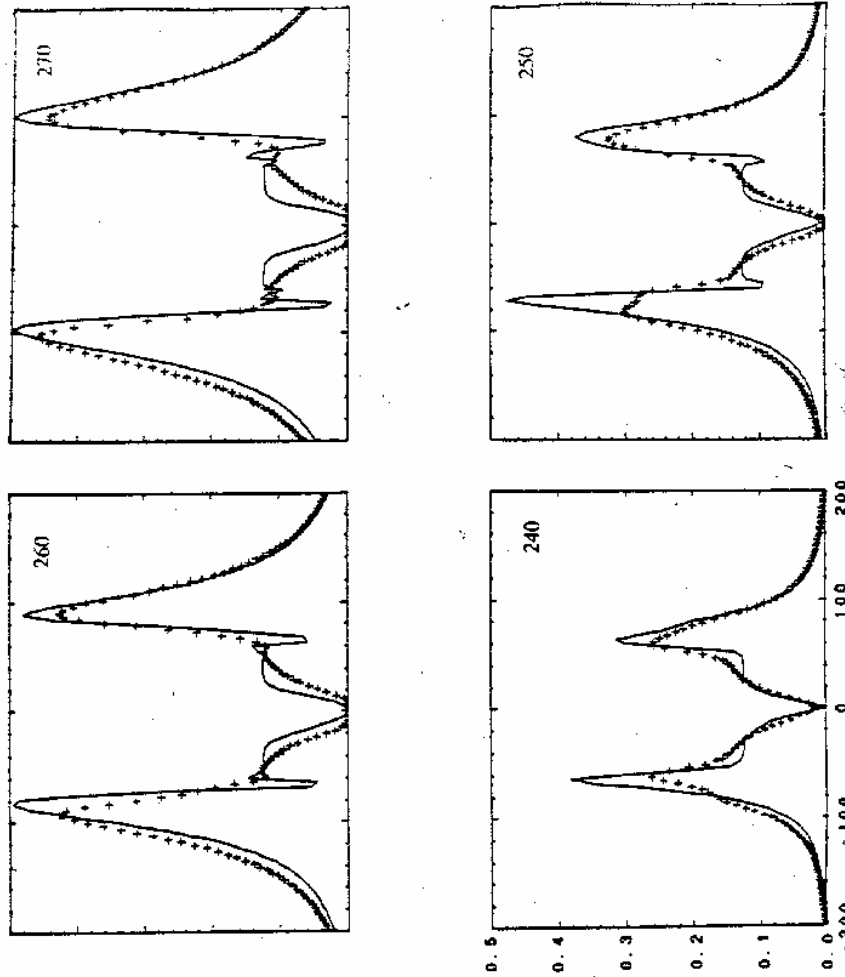
Fig.11b Same as 11a, but for the D$_2$ sodium line.
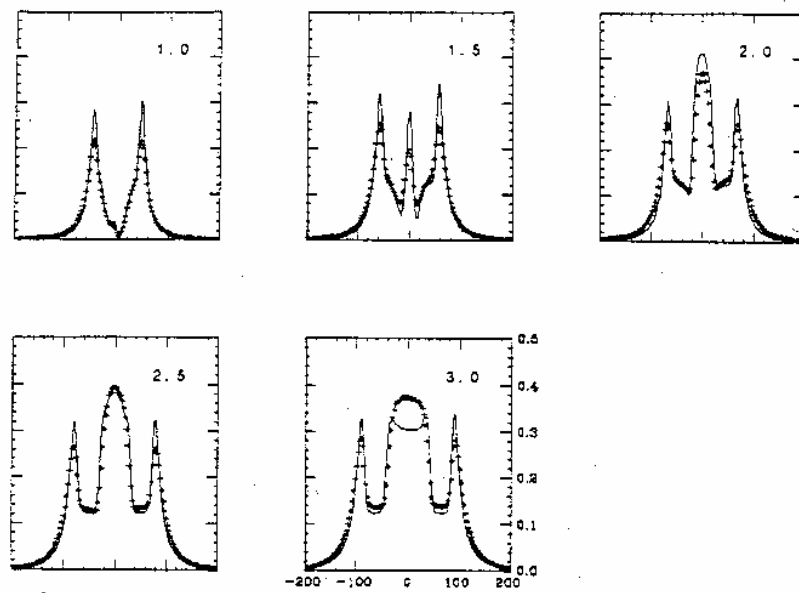
Fig.12 Calculated and measured (crosses) transmission funtions of the MOF for the D_1 sodium line. $T = 240°C$ and H varying from 1.0 to 3.0 Kgauss.

34
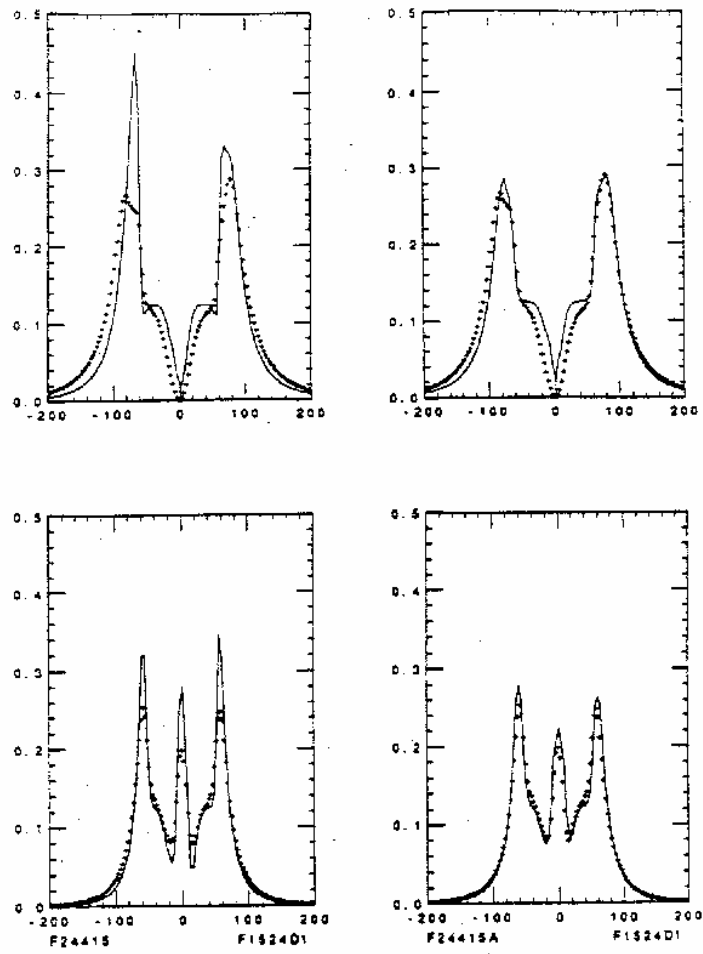
Fig.13 Comparison between spectral profiles calculated for a single light path (left) and averaged over a 8 mm diameter light beam (right).

35
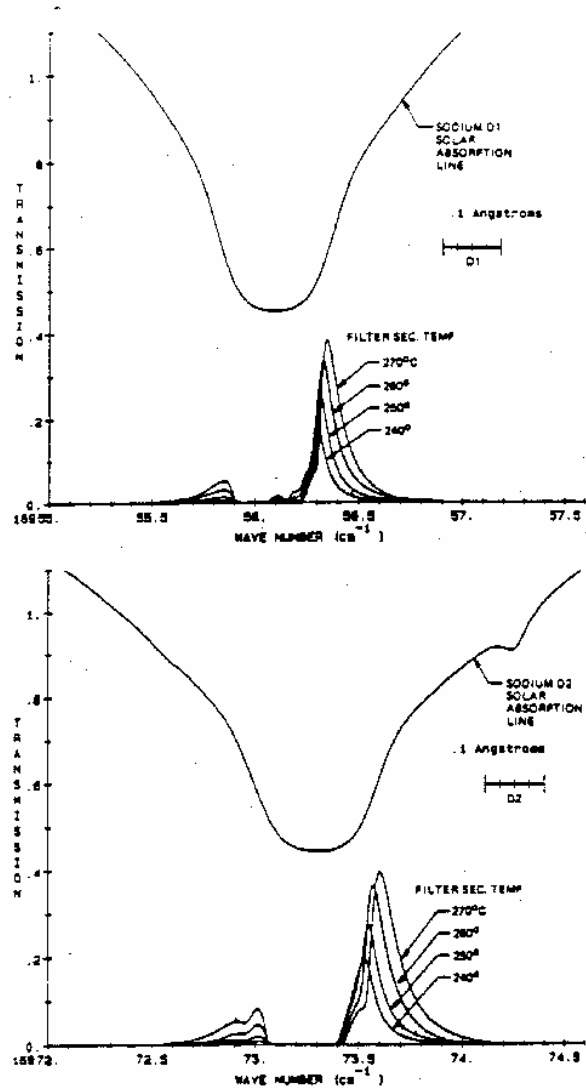
Fig. 14a Optimized measured MOF transmission profiles. Window losses are not included. (H$_F$=1 KG, HWS, T$_{WS}$ = 3 KG, 270° C). The solar profile has been displaced upward for better display.

36
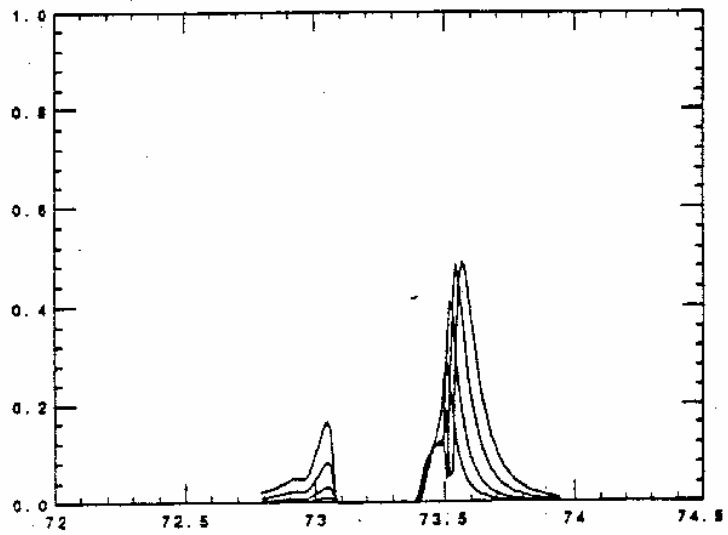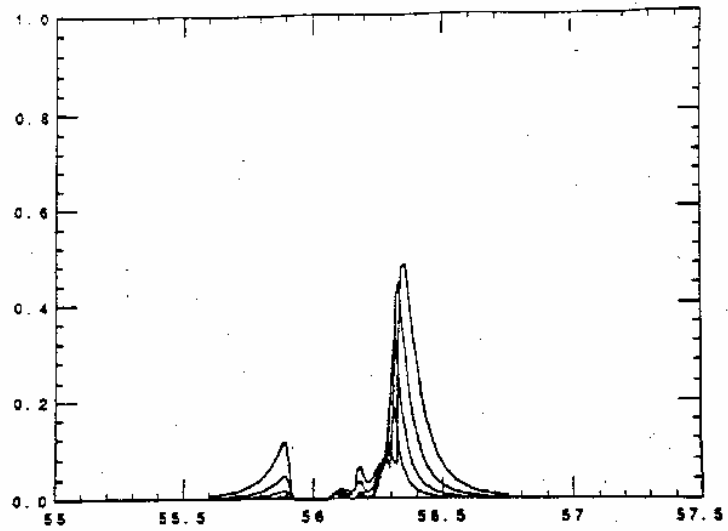
Fig. 14b MOF transmission profiles with the same parameters as 14a. The window losses are not included in the calculation.
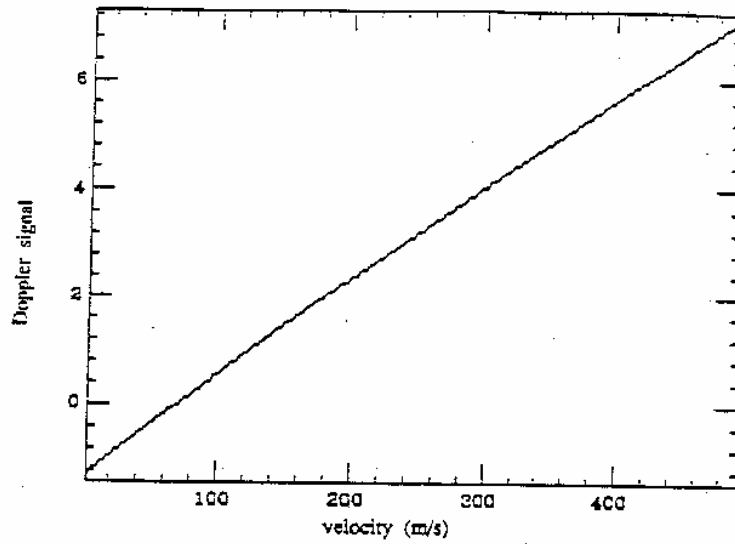
37

Fig. 15a   Diurnal variation of the velocity signal plotted against the radial earth-sun theoretical
velocity, v (see equation in text). Five minutes solar oscillations are clearly visible.
Data were taken on Nov. 8, 1990 at JPL. The MOF's spectral transmission was
optimized in order to have maximum sensitivity and stability. Note that there is an
"offset" (a null signal is equivalent to approximately 80 m/s) that can be caused by stray
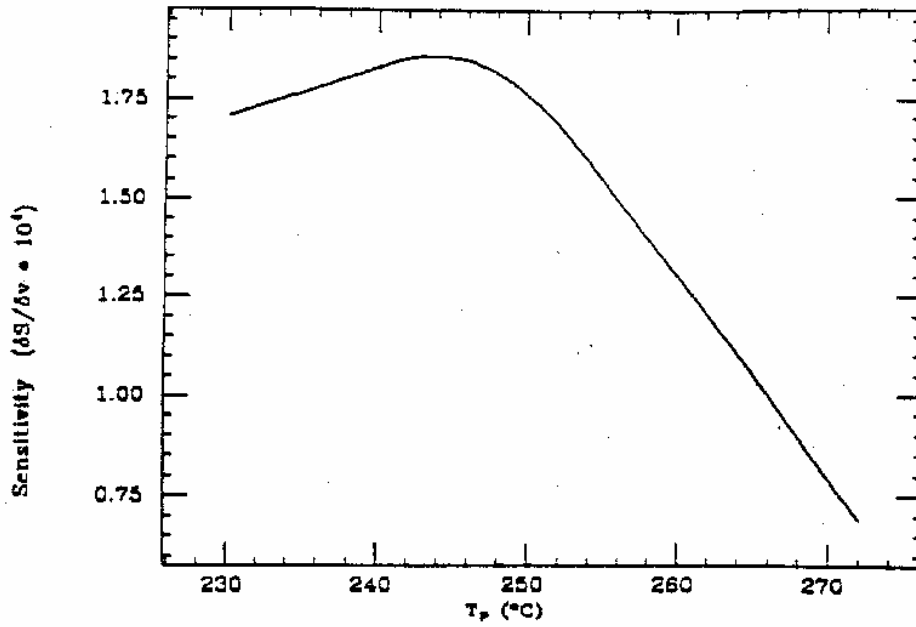polarization and asymmetries in the MOF response.

Fig. 15b Sensitivity (over a 4 Km/s dynamic range) MOF's response to the Doppler signal as a function of Filter's temperature. Same parameters as 14a.